IOPscience iopscience.iop.org

Home Search Collections Journals About Contact us My IOPscience

Thermal and electronic properties of amorphous $Al_{87}Y_8Ni_{5-x}TM_x$ (TM=Mn, Fe, Co, Cu)

This article has been downloaded from IOPscience. Please scroll down to see the full text article.

1992 J. Phys.: Condens. Matter 4 461

(http://iopscience.iop.org/0953-8984/4/2/014)

View the table of contents for this issue, or go to the journal homepage for more

Download details:
IP Address: 171.66.16.96
The article was downloaded on 10/05/2010 at 23:55

Please note that terms and conditions apply.

J. Phys.: Condens. Matter 4 (1992) 461–472. Printed in the UK

Thermal and electronic properties of amorphous $Al_{87}Y_8Ni_{5-x}TM_x$ (TM=Mn, Fe, Co, Cu)

M Yewondwossen†, R A Dunlap† and D J Lloyd‡

† Department of Physics, Dalhousie University, Halifax, Nova Scotia, Canada B3H 3J5

‡ Kingston Research and Development Centre, Alcan International Limited, Kingston, Ontario, Canada K7L 4Z4

Received 29 July 1991

Abstract. The thermal and electronic properties of amorphous $Al_{87}Y_8Ni_3TM_2$ (TM=Mn, Fe, Co, Ni, Cu) and $Al_{87}Y_8Ni_{5-x}Fe_x$ ($x = 0, 2, 3, 5$) alloys have been investigated. Thermal analysis studies have shown that all alloys studied here, except $Al_{87}Y_8Fe_5$, undergo a primary crystallization process which involves a precipitation of FCC-Al followed by a eutectic crystallization process to an intermetallic compound. $Al_{87}Y_8Fe_5$ undergoes eutectic crystallization directly and shows the highest crystallization temperature, 593 K, of the alloys studied here. Alloys which do not contain Fe show resistivities which are well described by the Ziman–Faber model for structurally disordered materials. Fe-containing alloys show electronic properties which suggest the influence of magnetic interactions. The magnitude and temperature dependence of the resistivity show compositional variations which can be related to thermal stability.

1. Introduction

The recent discovery [1, 2] of high tensile strength low density amorphous aluminum–rare-earth–transition metal (Al–RE–TM) alloys has prompted renewed research interest in rapidly solidified aluminum alloys for possible industrial applications. A major disadvantage of previously reported alloys of this type results from their poor thermal stability. The most commonly studied alloys of this type, Al–Y–Ni and Al–Ce–Fe, typically have tensile strengths in the range of 900–1100 MPa and Vickers hardness in the range of 300–400 diamond pyramid hardness (DPH) [3]. These may be compared with values of about 550 MPa and 180 DPH, respectively, for high strength crystalline Al-based alloys. Measured crystallization temperatures of the amorphous Al–RE–TM alloys which show the greatest tensile strength, $Al_{87}Y_8Ni_5$ and $Al_{89}Ce_5Fe_5$, are 488 K [4] and 543 K [5], respectively. In order to produce bulk amorphous materials by the consolidation of melt spun amorphous ribbons, it is necessary to improve substantially the thermal stability of these alloys without sacrificing mechanical strength. In order to approach this problem in a reasonable, systematic manner, it is important to have a thorough understanding of the fundamental physics of the crystallization mechanisms. In the present work, we have made a detailed study of the effects of transition metal substitutes on the crystallization processes in amorphous $Al_{87}Y_8Ni_5$. To supplement these results, we also report an investigation of the electrical resistivity of Al–Y–Ni

0953-8984/92/020461 + 12 $03.50 © 1992 IOP Publishing Ltd

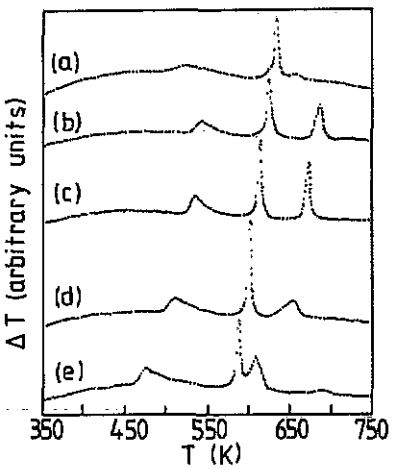

Figure 1. QDTA scans obtained at a heating rate of 20 K min^{-1} for $Al_{87}Y_8Ni_3TM_3$, with (*a*) TM=Mn, (*b*) TM=Fe, (*c*) TM=Co, (*d*) TM=Ni and (*e*) TM=Cu.

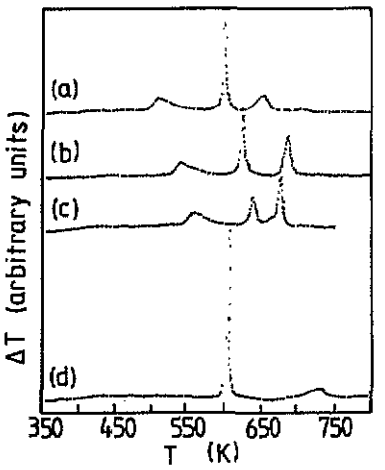

Figure 2. QDTA scans obtained at a heating rate of 20 K min^{-1} for $Al_{87}Y_8Ni_{5-x}Fe_x$ with (*a*) $x = 0$, (*b*) $x = 2$, (*c*) $x = 3$ and (*d*) $x = 5$.

based alloys. These relate microstructure and the details of electronic properties, and can help to clarify the relationship between TM content and crystallization mechanisms.

2. Sample preparation and experimental methods

Alloys of the following compositions were prepared for this study: $Al_{87}Y_8Ni_5$, $Al_{87}Y_8Ni_3TM_2$ (TM=Mn, Co and Cu) and $Al_{87}Y_8Ni_{5-x}Fe_x$ ($x = 2$, 3 and 5). These alloys were prepared in the fully amorphous form by arc melting high purity elemental components followed by melt spinning onto a single Cu roller. Quenching was performed under a helium atmosphere with a roller surface speed of 60 m s^{-1}. All as quenched alloys showed good ductibility.

Room temperature x-ray powder diffraction studies were performed on all samples using a Siemens D500 scanning diffractometer and CuK_α radiation. These showed no evidence for the presence of crystalline impurities in any of the as-quenched alloys. The homogeneous microstructure of these alloys was confirmed by transmission electron microscopy (TEM).

The measurement of the onset of crystallization and the heat of transformation was performed using a Fisher series 300 Quantitative Differential Thermal Analyzer (QDTA) with an Al_2O_3 reference standard. All QDTA samples had a mass of 25.0 ± 0.5 mg. Measurements were carried out over a temperature range from room temperature to about 800 K.

Electrical resistivity measurements were made between 4.2 K and room temperature, using a conventional 4–point DC method. Resistance measurements were accurate to about 1 part in 10^5.

Table 1. Results of QDTA measurements made at a heating rate of 20 K min^{-1} for amorphous $Al_{87}Y_8TM_5$ alloys. T_x is the temperature of the onset of crystallization in K and ΔH is the heat of transition in J kg^{-1}.

	Peak 1		Peak 2		Peak 3	
Alloy	T_x	ΔH	T_x	ΔH	T_x	ΔH
$Al_{87}Y_8Ni_3Mn_2$	498	0.017	610	0.067	—	—
$Al_{87}Y_8Ni_3Fe_2$	525	0.025	603	0.025	665	0.052
$Al_{87}Y_8Ni_3Co_2$	516	0.033	593	0.049	654	0.057
$Al_{87}Y_8Ni_5$	488	0.036	582	0.053	622	0.037
$Al_{87}Y_8Ni_3Cu_2$	454	0.036	567	0.103	667	0.007
$Al_{87}Y_8Ni_2Fe_3$	542	0.021	615	0.030	654	0.058
$Al_{87}Y_8Fe_5$	593	0.087	706	0.025	—	—

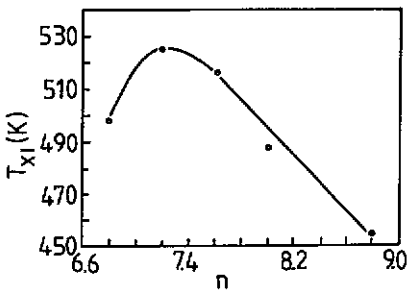

Figure 3. Onset temperature of the lowest temperature crystallization peak in $Al_{87}Y_8Ni_3TM_2$ as a function of the average number of 3d electrons per TM element.

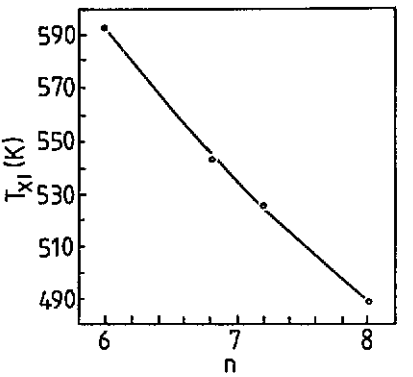

Figure 4. Onset temperature of the lowest temperature crystallization peak in $Al_{87}Y_8Ni_{5-x}Fe_x$ as a function of the average number of 3d electrons per TM element.

3. Results

3.1. Crystallization studies

Differential Thermal Analysis scans of all alloys studied here, as obtained with a heating rate of 20 K min^{-1}, are shown in figures 1 and 2. All scans show 2 or 3 crystallization peaks. The details of these peaks are given in table 1. Here, the QDTA provides a measure of the heat associated with each transition in terms of the area under the crystallization peak. The onset of crystallization is taken to be the temperature at which the temperature begins to deviate from the background.

It is interesting to consider the trends in the temperature of the onset of the lowest temperature crystallization peak as a function of the alloy composition. These trends are illustrated in figures 3 and 4. Clearly, for the $Al_{87}Y_8Ni_3TM_2$ series of alloys, there is a peak in T_{X_1} near Fe (average number of 3d electrons per TM, $n \sim 7.2$). It is therefore interesting to study the Al–Y–Ni–Fe system further and this is the motivation for

Table 2. Activation energies, in eV, obtained from the Kissinger method for heating rate between 5 K min^{-1} and 25 K min^{-1} for amorphous $Al_{87}Y_8TM_5$ alloys. Reliable data could not be obtained for $i = 1$ and $i = 3$ in TM=Mn alloy on account of poor peak resolution.

	E_i		
Alloy	Peak 1 ($i = 1$)	Peak 2 ($i = 2$)	Peak 3 ($i = 3$)
$Al_{87}Y_8Ni_3Mn_2$	—	3.1	—
$Al_{87}Y_8Ni_3Fe_2$	3.7	3.3	2.9
$Al_{87}Y_8Ni_3Co_2$	2.4	3.4	4.9
$Al_{87}Y_8Ni_5$	2.7	4.3	3.3
$Al_{87}Y_8Ui_3Cu_2$	2.1	3.1	2.5
$Al_{87}Y_8Ni_2Fe_3$	3.5	3.7	2.2
$Al_{87}Y_8Fe_5$	3.9	3.1	—

investigating $Al_{87}Y_8Ni_{5-x}Fe_x$ alloys as a function of x. As figure 4 shows, increasing x (i.e. decreasing n) increasing T_{X_1} substantially and T_{X_1} reaches a value of 593 K in $Al_{87}Y_8Fe_8$.

The details of the crystallization peaks of all alloys have been studied as a function of the heating rate used in the QDTA study. For different heating rates, $\gamma = dT/dt$, the measurement of the temperature of the peak of the crystallization exotherm, T_{Pi}, allows for the calculation of the activation energy of the processes responsible for the ith peak, E_i. Data obtained in this way are analysed according to the Kissinger method [4, 6]. This gives the relationship between γ and T_{Pi} as

$$d[\ln(\gamma/T_{Pi}^2)]/d[1/T_{Pi}] = -E_i/k \tag{1}$$

where k is Boltzman's constant. The slope of the data for $-\gamma/T_{Pi}^2$ as a function of $1/T_{Pi}$ gives the activation energy. Typical data of this type are illustrated in figure 5. Activation energies obtained in this way are given in table 2.

Information concerning the microscopic details of the crystallization processes can be determined on the basis of the method of Ozawa [7, 8]. In this case, the fraction transformed as a function of heating rate, (γ), was determined by the relative area of a crystallization peak up to a temperature, T_d, since

$$d\{\log[\ln(1 - x(\gamma))]\}/d \log \gamma|_{T_d} = -n \tag{2}$$

where n is the Avrami exponent and is an important factor in determining the mode of crystallization. The temperature T_d is chosen to be on the high temperature tail of the crystallization exotherm as measured using the slowest heating rate (5 K min^{-1}). Measured values of n for the alloys investigated here are given in table 3.

We have studied the crystallization products of the present alloys. As typical examples of information gained from these studies, we discuss the results for $Al_{87}Y_8Ni_5$ and $Al_{87}Y_8Fe$. The $Al_{87}Y_8Ni_5$ alloy has been heated to temperatures above each of the three crystallization exotherms. The x-ray patterns of the samples prepared in this way are illustrated in figure 6. The lowest temperature exotherm is seen to correspond to the precipitation of FCC-Al. This is similarly the case for all other alloys studied here, except for the $Al_{87}Y_8Fe_5$ alloy. Figure 6 shows that the second exothermic peak corresponds to the precipitation of additional FCC-Al and a further decrease in the amorphous

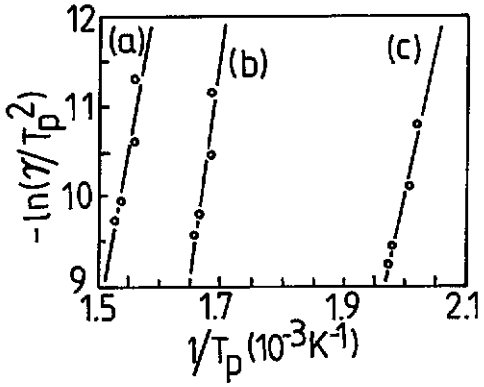

Figure 5. Kissinger plots for amorphous $Al_{87}Y_8Fe_5$: (*a*) $i = 1$ (peak 1), (*b*) $i = 2$ (peak 2) and (*c*) $i = 3$ (peak 3).

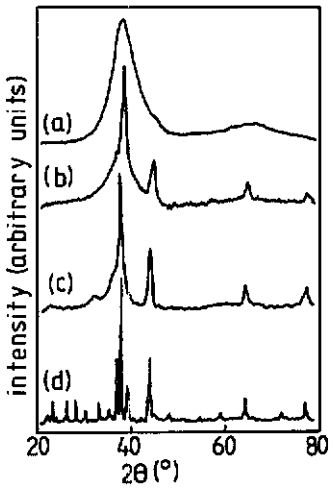

Figure 6. X-ray diffraction patterns (CuK_α) of $Al_{87}Y_8Ni_5$: (*a*) as-quenched, (*b*) after heating to a temperature just above the first exotherm, (*c*) after heating to a temperature just above the second exotherm and (*d*) after heating to a temperature just above the third exotherm.

Table 3. Measured Avrami exponents, *n*, associated with the different crystallization peaks in amorphous $Al_{87}Y_8TM_5$ alloys. Values of *n* are ±0.4. Some peaks were too weak to yield reliable results.

	n		
Alloy	Peak 1	Peak 2	Peak 3
$Al_{87}Y_8Ni_3Mn_2$	0.9	1.6	—
$Al_{87}Y_8Ni_3Fe_2$	0.9	2.5	4.1
$Al_{87}Y_8Ni_3Co_2$	0.9	2.5	6.1
$Al_{87}Y_8Ni_5$	1.0	2.6	2.1
$Al_{87}Y_8Ni_3Cu_2$	0.7	0.9	—
$Al_{87}Y_8Ni_2Fe_3$	1.4	2.4	4.8
$Al_{87}Y_8Fe_5$	3.7	1.7	—

component. This again is similar in all other alloys studied here, except for $Al_{87}Y_8Fe_5$. The third exotherm corresponds to the crystallization of the remaining amorphous component of the sample. The final crystallization product for $Al_{87}Y_8Ni_5$ is primarily FCC-Al. There is also a minor component of a binary or ternary intermetallic phase which could not be identified.

The $Al_{87}Y_8Fe_5$ alloy, unlike all other alloys studied here, showed a large first exothermic peak in the QDTA. In order to ensure that a small precursor of this crystallization process did not occur, we have studied a sample of this alloy which was heated to just below the onset temperature of 593 K (i.e. 570 K). X-ray diffraction patterns of this and other annealed samples of $Al_{87}Y_8Fe_5$ are shown in figure 7. No measurable crystallization

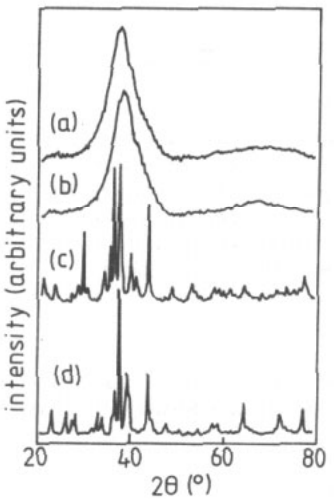

Figure 7. X-ray diffraction patterns (CuK_α) of $Al_{87}Y_8Fe_5$: (*a*) as-quenched, (*b*) after heating to 570 K (just below the first exotherm), (*c*) after heating to a temperature just above the first exotherm and (*d*) after heating to a temperature just above the second exotherm.

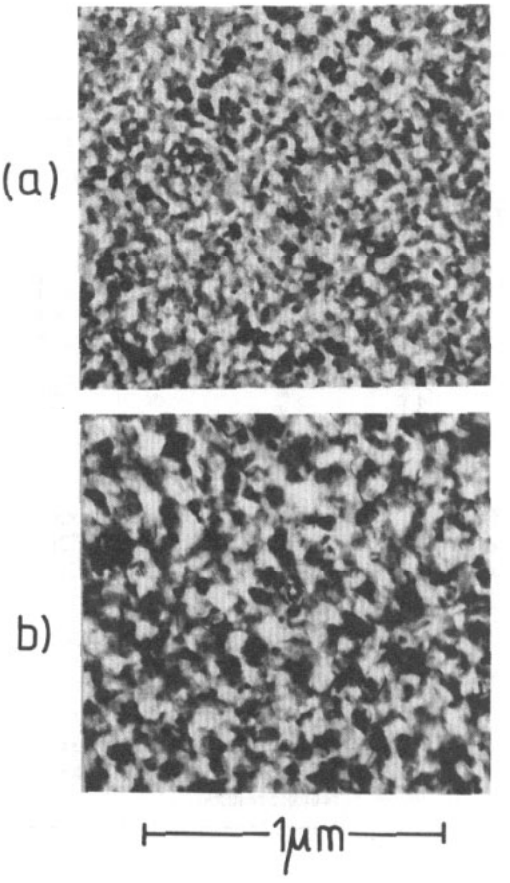

Figure 8. Transmission electron microscope (TEM) pictures of $Al_{87}Y_8Fe_5$ heated to (*a*) just above the first exotherm and (*b*) just above the second exotherm. These correspond to the x-ray patterns of figures 7*c* and 7*d*, respectively.

is seen in the sample heated to 570 K, although minor changes in the high angle portion of the diffuse scattering pattern indicates that annealing has produced some structural relaxation of the amorphous phase. As figure 7 shows, the main crystallization exotherm corresponds to the formation of FCC-Al and an unidentified intermetallic phase. At this point there is no measurable amorphous component remaining. The higher temperature exotherm corresponds to a crystallographic transition of the intermetallic phase with little change in the FCC-Al component of the alloy. Changes in the structural morphology during these processes are readily seen using transmission electron microscopy (TEM). TEM images of as-quenched amorphous alloys show a homogeneous alloy with no detectable grain structure. Figure 8 shows TEM images of $Al_{87}Y_8Fe_5$ obtained after heating above each of the two exothermic peaks. Figure 8(*a*) shows the formation of crystalline grains which occur during the first exotherm reaction, and figure 8(*b*) shows that substantial grain growth occurs during the second exothermic reaction.

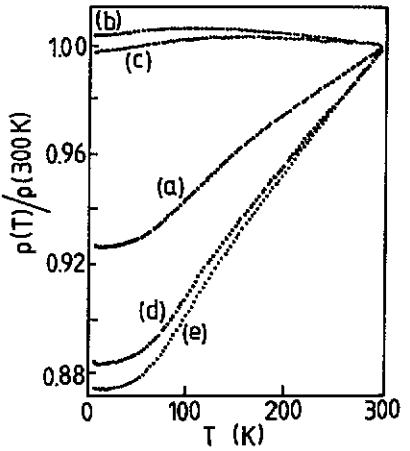

Figure 9. Normalized electrical resistivity as a function of temperature for amorphous $Al_{87}Y_8Ni_3TM_2$ for (*a*) TM=Mn, (*b*) TM=Fe, (*c*) TM=Ni, (*d*) TM=Co and (*e*) TM=Cu.

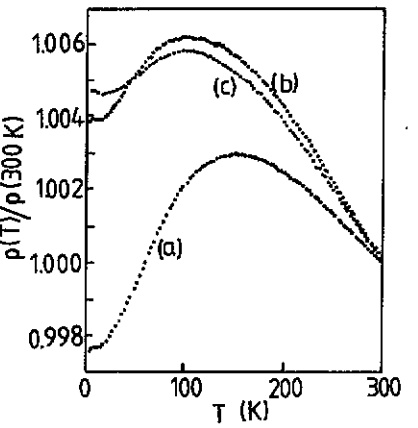

Figure 10. Normalized electrical resistivity as a function of temperature for amorphous $Al_{87}Y_8Ni_{5-x}Fe_x$ for (*a*) $x = 0$, (*b*) $x = 2$ and (*c*) $x = 5$.

Table 4. Resistivity parameters for amorphous $Al_{87}Y_8TM_5$ alloys. Absolute ρ measurements are ±3%.

Alloy	ρ(300 K) [$\mu\Omega$ cm]	$(1/\rho)(\partial\rho/\mu T)_{T=300K}$ ($\times 10^{-4}$ K^{-1})
$Al_{87}Y_8Ni_3Mn_2$	87	+2.6
$Al_{87}Y_8Ni_3Fe_2$	78	−32.9
$Al_{87}Y_8Ni_3Co_2$	78	+4.8
$Al_{87}Y_8Ni_5$	71	−18.2
$Al_{87}Y_8Ni_3Cu_2$	65	+4.5
$Al_{87}Y_8Mo_3Fe_3$	83	+223.0
$Al_{87}Y_8Fe_5$	91	−34.4

3.2. Electrical resistivity studies

Normalized resistivity curves, $\rho(T)/\rho(300\text{ K})$, for all alloys studied here are shown in figures 9 to 11. Details of absolute ρ measurements at 300 K are given in table 4.

The evaluation $\rho(T)$ on the basis of any well defined theory is not straightforward. In disordered materials, the high temperature regime is the easiest to deal with. On the basis of the Faber–Ziman theory as subsequently developed by Meisel and Cote [9–11], the resistivity of a material is proportional to the structure factor, $S(k)$, where k is the phonon wave vector. For temperatures $T \geqslant \theta_D/2$ (θ_D is the Debye temperature) the structure factor may be expressed as [5]

$$S(k) = bT \tag{3}$$

where b is a constant. The resistivity is therefore expressed as a linear function of temperature as [5]

Table 5. Parameters obtained from fits to Ziman–Faber theory for normalized resistivity of $Al_{87}Y_8Ni_3TM_2$ (TM=Mn, Co, Cu) alloys. See equations (4) and (6).

TM	a_1	a_2 (10^{-6} K^{-2})	b_1	b_2 (10^{-4} K^{-1})	θ_D (K)
Mn	0.93	1.9	0.92	2.6	260
Co	0.87	3.8	0.86	4.8	240
Cu	0.89	3.5	0.87	4.5	240

Table 6. Parameters obtained from fitting low temperature normalized resistivity data for $Al_{87}Y_8Ni_{5-x}Fe_x$ to equation (7).

x	a_1	a_2 (K$^{-3/2}$)
0	70.56	388
2	78.46	328
3	75.49	2012
5	91.80	187

$$\rho(T)/[\rho(300\text{ K})] = b_1 + b_2T. \tag{4}$$

The low temperature regime is more problematic. For $T \leqslant \theta_D/2$, Meisel and Cote [9] have expressed the structure factor as

$$S(k) = 1 + aT^2. \tag{5}$$

This gives a resistivity as

$$\rho(T)/\rho(300\text{ K}) = a_1 + a_2T^2. \tag{6}$$

Along somewhat different lines, theoretical treatments of magnetic scattering at low temperatures, [12 e.g.], predicted a low temperature dependence

$$\rho(T)/\rho(300\text{ K}) = a_1 + a_2T^{3/2}. \tag{7}$$

A computer analysis of the present data has shown that the low temperature behaviour of the resistivity is best fitted to equation (6) for the $Al_{87}Y_8Ni_3TM_2$ (TM=Mn, Co, Cu) alloys and to equation (7) for the $Al_{87}Y_8Ni_{5-x}Fe_x$ ($x = 0, 2, 3, 5$) alloys.

The alloys which are well described by Ziman–Faber theory at low temperatures show a well defined linear dependence of the resistivity at high temperatures. An estimate of the Debye temperature is made on a basis of temperature ranges for which various fitting methods are applicable. Results of such an analysis are shown in table 5. For the low temperature region ($T \leqslant 100$ K) fits to equation (7) for the $Al_{87}Y_8Ni_{5-x}Fe_x$ series ($x = 0, 2, 3, 5$) have yielded parameters given in table 6.

4. Discussion

From a practical standpoint, we have seen that $Al_{87}Y_8Fe_5$ shows a substantially greater crystallization temperature than other Al-based amorphous alloys that have been

reported previously. This alloy also retains good ductility. This, in itself, signifies a significant advance in the ability to utilize amorphous Al-based alloys for commercial applications. The present systematic study also provides some insight into the relationship of crystallization processes and the fundamental physical properties of amorphous Al-based alloys.

Although many Fe-based amorphous alloys exhibit crystallization temperatures which can be linearly related to the mean TM atomic radius [13], this is not a universal phenomenon [14]. In the present study, it is seen from figure 3 that a linear relationship between crystallization temperature and TM radius does not exist.

In a phenomenological manner [15], the decrease in T_c observed in figure 3 for TM to the left of Fe can be explained by a decrease in viscosity of the liquid alloy and a corresponding increase in diffusivity. Nagel and Tauc have quantified the description of amorphous alloy stability in terms of the electronic structure [16] in the following way: the stability of an amorphous phase is maximized when the Fermi energy is at a minimum in the density of states (DOS). This condition is satisfied when

$$2k_F = k_P \tag{8}$$

where $2k_F$ is the diameter of the free electron Fermi sphere and $2k_P$ is the wave vector associated with the first diffuse peak in the structure factor, $S(k)$. Of particular relevence to the measurements presented here is the factor that when equation (8) is satisfied the temperature coefficient of the electrical resistivity (TCR) will be negative at room temperature. In many amorphous alloys such a correlation has been observed between T_x and the TCR, e.g. [17, 18].

For the results presented here for the $Al_{87}Y_8Ni_3TM_2$ alloys, a comparison of T_x and the value of the TCR from tables 1 and 4 indicates that the most negative TCR (for TM=Fe) corresponds to the most stable alloy in this series. Again, for all the $Al_{87}Y_8Ni_{5-x}Fe_x$ series of alloys, the measurements presented here indicate that the alloy with the most negative TCR (i.e. $Al_{87}Y_8Fe_5$) also has the highest T_x.

X-ray diffraction studies of Al–Y–Ni–TM alloys have shown no measurable systematic change in k_P. Variations in T_x which correspond to changes in the DOS at the Fermi energy in the $Al_{87}Y_8Ni_3TM_2$ alloys presumably correspond primarily to changes in $2k_F$ which result from changes in the 3d electron concentration in the alloys. From figure 3, we see that this occurs near TM=Fe for this alloy series. For TM on either side of Fe, the condition of equation (8) no longer holds and a corresponding decrease in T_x and a more positive TCR occur.

Since all annealed alloys which showed the presence of crystalline phases exhibited diffraction patterns corresponding to Al or Al and one or more intermetallic phases, the crystallisation reactions in all alloys studied here do not represent polymorphic crystallization of an amorphous phase to an intermetallic phase of the same composition. In all alloys except $Al_{87}Y_8Fe_5$, the lowest temperature exothermic reaction corresponds to the precipitation of FCC-Al within the amorphous phase. This process obviously corresponds to primary crystallization. Further heating of these samples resulted in the formation of an unidentified crystalline phase from the remaining amorphous component of the alloy. This behaviour, along with the morphology of the microstructure, as seen by TEM studies, indicates that the second exothermic reaction in all alloys (except $Al_{87}Y_8Fe_5$) is the result of a eutectic crystallization process. This is also true of the first exothermic peak for $Al_{87}Y_8Fe_5$.

The general relationship between alloy stability and the activation energy associated with the first crystallization exotherm is clearly seen by a comparison of T_x from table 1

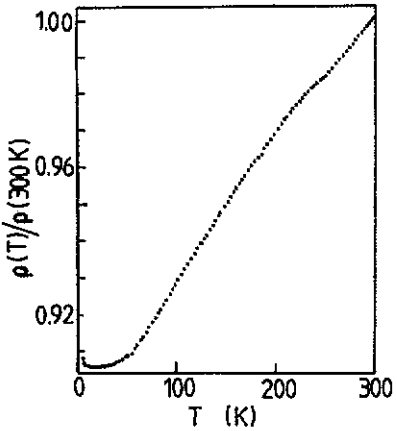

Figure 11. Normalized electrical resistivity as a function of temperature for amorphous $Al_{87}Y_8Fe_5$.

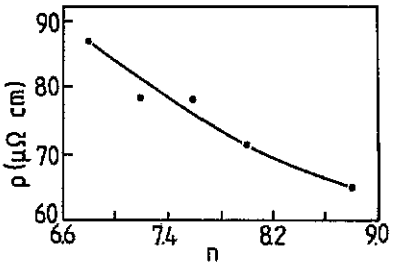

Figure 12. Room temperature resistivity, ρ, as a function of the average 3d electron concentration per TM atom in amorphous $Al_{87}Y_8Ni_3TM_2$ (TM=Mn, Fe, Co, Ni, Cu) alloys.

and E_1 from table 2. For the $Al_{87}Y_8Ni_3TM_2$ series, both of these quantities have a maximum at TM=Fe and for the $Al_{87}Y_8Ni_{5-x}Fe_x$ both have a maximum for $x = 0$. This suggests a relationship between a decrease in atomic mobility, as evidenced by an increase in E_1 during crystallization and an increase in the thermal stability of the alloy.

The kinetics of primary crystallization involves long-range atomic transport and the details of the Avrami exponent, n, allow for a qualitative understanding of the processes responsible for crystallization. The effective Avrami exponent is given in terms of growth and nucleation components, n_g, and n_n, respectively, as

$$n = n_g + n_n \tag{9}$$

where the total n is $1.5 \leqslant n < 4.0$. When $0 < n < 1$, the process is nucleation dominated and when $1.5 < n < 4$ then the process is growth dominated [7]. From table 3, the n values for the first crystallization exotherm of all alloys (except $Al_{87}Y_8Fe_5$) are around unity. This suggests that both nucleation of crystallization sites and the growth of quenched-in nucleation sites play a role in the primary crystallization of these alloys. As we would anticipate, the much larger typical values of n for the second and third exothermic reactions in these alloys indicates that they are essentially growth dominated processes.

For the $Al_{87}Y_8Fe_5$ alloy, the Avrami exponent for the first crystallization peak, $n = 3.7$, is characteristic of a eutectic crystallization process. Ideal eutectic crystallization accompanied by uniform three dimensional growth yields $n = 3$. On the other hand, a constant eutectic nucleation rate and a linear growth rate in three dimensions would give $n = 4$. The result obtained here is certainly consistent with eutectic crystallization but the distinction between the two possibilities given here is not entirely clear.

The results of the resistivity studies presented here can provide additional important information concerning the physical properties of these alloys, in terms of the following behaviour, as discussed below: (i) Ziman–Faber behaviour; (ii) the effects of 3d electron concentration on ρ; (iii) effects of magnetic interactions on ρ in Fe-containing alloys; and (iv) a consideration of ρ and the TCR in the context of the Mooij correlation [19].

The observed temperature dependence of ρ in $Al_{87}Y_8Ni_3TM_2$ (TM=Mn, Co, Ni, Cu) have been appropriately described by a T^2 dependence below $\theta_D/2$ and a linear T-dependence above about $\theta_D/2$. The Ziman–Faber theory [11, 12] models this behaviour on the basis of conduction electron scattering which is primarily due to structural scattering from the dense random atomic packing of the amorphous phase. In this treatment, it is shown that the coefficient of the linear term at high T, as well as the absolute value of the resistivity, are highly sensitive functions of the relative values of $2k_F$ and k_p. High resistivity values are a consequence of the condition given by equation (8) and phenomenologically this corresponds to an atomic microstructure which is particularly effective at scattering conduction electrons. The room-temperature resistivity may be expressed as [20, 21]

$$\rho \propto S(2K_f)2\Gamma^2/[\Gamma^2 + 4(E_r - E_F)^2] \tag{10}$$

where Γ is the width, E_r is the energy of the scattering resonance (which lies near the centre of the 3d band) and E_F is the Fermi energy. From (10), we see that there are two contributions to ρ: scattering related to the structure factor, $S(k)$ and resonant scattering related to $(E_r - E_F)$. Since $S(k)$ is similar for all 3d transition metals, differences in ρ are primarily due to differences in $(E_r - E_F)$ [21]. As Mn has a half-filled 3d band, the number of 3d electrons, and hence E_F, increases from Mn to Cu across the 3d series. This means that $(E_r - E_F)$ also increases and ρ decreases with increasing numbers of 3d electrons. This same trend is seen in transition metal glasses with 3d addition and is seen as well for the present $Al_{87}Y_8Ni_3TM_2$ alloys, as illustrated in figure 12.

The alloy with the greatest thermal stability, $Al_{87}Y_8Fe_5$, also shows the most negative TCR. This is readily shown to be consistent with the condition of equation (8). As the temperature is increased, the peak in $S(k)$ broadens. Thus the number of atomic pairs for which maximum scattering occurs will decrease. This yields a corresponding decrease in ρ.

The large room temperature values of ρ are also consistent with the condition of equation (8). In pure TMs, $2k_F$ lies well below k_p. The addition of a sizeable fraction of highly valent atoms (in this case, Al) increases $2k_F$ and shifts the Fermi diameter towards the peak in $S(k)$. This increases the structure factor contribution to the resistivity, as shown in equation (10), and increases ρ. This behaviour can be seen to be characteristic of the measurements obtained from both the $Al_{87}Y_8Ni_3TM_2$ series and the $Al_{87}Y_8Ni_{5-x}Fe_x$ series of alloys.

The $Al_{87}Y_8Ni_{5-x}Fe_x$ alloys are characterized by electronic behaviour that is typical of systems in which magnetic interactions play an important role in electron scattering. In alloys which exhibit spin glass freezing as a result of dilute magnetic impurities, the electrical resistivity shows a $T^{3/2}$ temperature dependence at low temperature and a linear T-dependence with a negative TCR at high temperatures. Although the general features of the resistivity observed in the $Al_{87}Y_8Ni_{5-x}Fe_x$ alloys can be explained in terms of the behaviour described above, long-lived elementary excitations [22] can yield similar behaviour. Detailed magnetic susceptibility studies will be necessary to clarify the behaviour of these alloys.

5. Conclusions

We have shown that, by a careful consideration of the composition of Al-rich amorphous alloys, their thermal stability can be substantially improved. The suppression of primary

crystallization processes for certain stoichiometries plays an important role in increasing the crystallization temperature. It has been shown that the electronic transport properties are closely related to thermal stability and that theoretical considerations based on the disordered nature of amorphous alloys are important for an understanding of the electron scattering mechanisms in these alloys. This, in turn, can lead to an understanding of those fundamental aspects of the electronic structure which are most relevant to improving thermal stability. While we have presented the results of a study involving only a small portion of the Al–Y–TM phase diagram, we have illustrated that such investigations can be informative and productive.

Acknowledgment

This work was supported by grants from the Natural Sciences and Engineering Research Council of Canada.

References

[1] He Y, Poon S J and Shiflet G J 1988 *Science* **241** 1640
[2] Inoue A, Ohtera K and Masumoto T 1988 *Japan. J. Appl. Phys.* **27** L736
[3] Inoue A, Ohtera K and Masumoto T 1988 *Japan. J. Appl. Phys.* **27** L479
[4] Yewondwossen M H 1990 *MSc Thesis* Dalhousie University (unpublished)
[5] Dunlap R A, Yewondwossen M H, Srinivas V, Christie I A, McHenry M E and Lloyd D J 1956 *J. Phys.: Condens. Matter* **2** 4315
[6] Kissinger H E 1956 *J. Res. NBS* **57** 217
[7] Christian J W 1975 *Theory of Transformations in Metals and Alloys* (London: Pergamon)
[8] Ozawa T 1971 *Polymer* **12** 150
[9] Meisel L V and Cote P 1977 *Phys. Rev.* B **16** 2978
[10] Ziman J M 1961 *Phil. Mag.* **6** 1014
[11] Faber T E and Ziman J M 1965 *Phil. Mag.* **11** 153
[12] Edwards S F and Anderson P W 1975 *J. Phys. F: Met. Phys.* **5** 965
[13] Walter J L 1981 *Mater. Sci. Eng.* **50** 137
[14] Masumoto T, Naka M, Tomizawa S and Watanabe T 1976 *Proc. 2nd Int. Conf. Rapidly Quenched Metals* ed N J Grant and B C Giessen (Cambridge, MA: MIT) p 273
[15] Coleman E 1976 *Mater. Sci. Eng.* **23** 161
[16] Nagel S R and Tauc J 1975 *Phys. Rev. Lett.* **35** 380
[17] Cote P J and Meisel L V 1978 *Proc. 3rd Int. Conf. Rapidly Quenched Metals* vol 1, ed B Cantor (London: The Metals Society) p 383
[18] Pekala K and Trykozoko R 1980 *Appl. Phys.* **22** 369
[19] Mooij J H 1973 *Phys. Status Solidi* a **17** 521
[20] Suryanarayama C 1984 *Metallic Glasses; Production, Properties and Applications* ed T R Anantharaman (Zurich: Trans. Technical) p 249
[21] Chen H S 1980 *Rep. Prog. Phys.* **43** 353
[22] Choudhury D and Mookerjee A 1984 *Phys. Rep.* **114** 1